tion measured on the Landsat imagery. Each break in the line represents a point along the coast where relatively straight trends within one of the larger arcs intersect.

The distribution of rates of shoreline change and orientation (Fig. 3) indicates that the erosional and storm-overwash areas are associated with the configuration of the island. In most cases, the closer the shoreline trends approach a north-south orientation, the greater the recession rates. We further tested with correlation the relationship between orientation of segments and mean recession rates for each segment. We were able to define 15 segments along Assateague from a Landsat II imagery enlargement of 1:80,000. The correlation coefficient (r) between coastal orientation (degrees north of east) and shoreline recession (mean + 1 S.D., meters per year) was .44. When nine segments were defined from a smaller-scale enlargement of 1:250,000, r increased to .94 (Fig. 3). It is clear that when the scale of a Landsat enlargement is increased, smaller crescentic features appear which are not related to the mesoscale processes and the correlation coefficient is reduced.

We performed the same tests for the barrier islands of North Carolina; however, the shoreline trend of the Outer Banks changes abruptly at Cape Hatteras, so the islands were stratified into three reaches—Ocracoke, South Hatteras, and North Hatteras (Fig. 1). Ocracoke, like Assateague, shows very high correlation (r = .94) between orientation and shoreline recession. The correlation for South Hatteras drops to r = .49, and North Hatteras has the weakest correlation (r = .39).

These areas are all in the same climatic regime, so the process-response relationships should be similar. With the exception of an occasional hurricane, winter extratropical storms cause the most widespread coastal change along the mid-Atlantic. As these storms move northeast with wind fields circulating counterclockwise, the highest and most damaging waves approach the coast from the northeast. The mean orientation for North Hatteras is 183.5°, for Assateague 156.5°, for Ocracoke 121.5°, and for South Hatteras 107.6°, all degrees north of south. There appears to be a high-energy orientation window centered around the northeast. If segments of the mid-Atlantic coast have this orientation, the rate of erosion and distance of storm-surge penetration along those segments increase (Fig. 4).

Included within our test site are engineering structures that greatly alter the inshore sediment transport processes. For example, the northern 10 km of Assateague Island have been rapidly eroding since the Ocean City inlet jetties were built in 1933—the rate has been approximately 12 m/year since 1934. Since this island segment is not undergoing natural change, when it was eliminated from our tests r increased to .99.

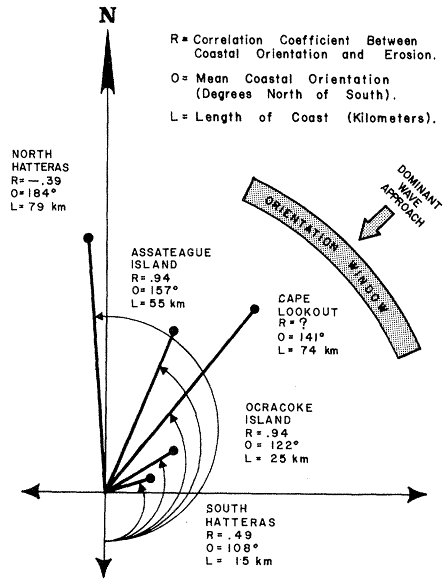

Fig. 4. Orientation and erosion statistics for five major segments of mid-Atlantic barrier islands. This polar coordinate plot of the mean orientation of the mid-Atlantic coast barrier islands suggests that there is an orientation window due approximately northeast. If the mean orientation of a large section of sedimentary coast is found, then the following relationship holds: as smaller straight-line segments of large crescentic or arcuate patterns of that coastal section approach a more north-south orientation (as they lie more perpendicular to the dominant wave approach) the rate of erosion increases.

We conclude that shoreline configuration is functionally related to organized mesoscale processes within the inshore zone and that the fluid motions responsible for large-scale crescentic shoreline forms are consistent along the mid-Atlantic coast. Our results are also consistent with Davies' (*3*) description of orientations in swell-dominated coasts. However, on complex storm-dominated coasts a greater along-the-coast variation in wave transformation processes appears to determine equilibrium configuration.

ROBERT DOLAN
BRUCE HAYDEN
JEFFREY HEYWOOD
Department of Environmental Sciences, University of Virginia, Charlottesville 22903
LINWOOD VINCENT
Waterways Experiment Station, U.S. Army Corps of Engineers, Vicksburg, Mississippi 39180

References and Notes

1. R. Dolan, *Geol. Soc. Am. Bull.* **82**, 177 (1971).
2. D. J. P. Swift, D. B. Duane, T. McKinney, *Mar. Geol.* **15**, 227 (1974).
3. J. L. Davies, *Geographical Variation in Coastal Development* (Hafner, New York, 1973).
4. R. T. Guza and D. L. Inman, *J. Geophys. Res.* **88**, 2997 (1975); M. S. Longuet-Higgins, in *Waves on Beaches*, R. E. Meyer, Ed. (Academic Press, New York, 1972), pp. 203–248; C. J. Sonu, *J. Geophys. Res.* **77**, 3232 (1972); A. J. Bowen, *ibid.* **76**, 8662 (1971); D. J. P. Swift, in *Marine Sediment Transport and Environmental Management*, D. J. Stanley and D. J. P. Swift, Eds. (Wiley, New York, 1976), pp. 255–310.
5. P. D. Komar, *Geol. Soc. Am. Bull.* **82**, 2643 (1971); M. S. Longuet-Higgins and D. W. Parkin, *Geogr. J.* **128**, 194 (1962); C. J. Sonu, *J. Geol.* **81**, 42 (1973).
6. R. Dolan and J. C. Ferm, *Science* **159**, 627 (1968).
7. R. Dolan, L. Vincent, B. Hayden, *Z. Geomorphol.* **18**, 1 (1974).
8. This work was supported by NASA contract NAS5-20999, NASA Wallops Island, and the National Park Service.

8 November 1976; revised 8 February 1977

Somali Current: Recent Measurements During the Southwest Monsoon

Abstract. *The Somali Current was measured at approximately maximum strength for the year during the southwest monsoon on 11 and 12 August 1975 (approximately $1^1/_2$ days) at stations spaced 20 to 35 kilometers apart. These measurements permit a nearly synoptic detailed mapping of the temperature structure of a major western boundary current.*

The Somali Current occurs seasonally, developing during the southwest monsoon in the Indian Ocean approximately between May and September each year. It flows northeast along the East African coast between about 4°S and 12°N and reaches its greatest velocity during July and August near 5°N to 10°N, where speeds of up to 350 cm/sec at the surface have been observed (*1*). The directly measured volume transport during that time was 62 × 10^6 m^3/sec in the upper 200 m across a section 350 km wide. Although the current is comparable to the Gulf Stream or the Kuroshio, it is relatively shallow (upper 200 to 400 m) and appears to be basically wind-driven. Surveys of the circulation off the Somali coast show that the current turns strongly offshore eastward and can be associated with one or more large eddies ranging up to 600 km or more across (*2*). Where the flow turns offshore, a region of cold upwelled water is found that extends seaward as a cold trough bounding the left side of the current. Our previous observations indicated that the circulation is relatively unstable, with noticeable changes in the size and location of the eddy structure occurring over a period of 1 month (*3*). Because of these changes and because of the large area encompassed by the circulation, past surveys have required 1 to 2 months to complete and have resulted in a somewhat distorted description of the current structure.

Recently, with the cooperation of relatively fast U.S. Navy ships that were on deployment in the Indian Ocean, we were able to obtain a nearly synoptic temperature survey of the coastal portion of the Somali Current during about a 1½-day period on 11 and 12 August 1975. The current at this time would be expected to be at nearly maximum strength. Expendable bathythermograph (XBT) probes (depth range, 0 to 450 m; type T-4, Sippican Corp.) were released at each measurement station. The four ships proceeded abreast northeasterly downcurrent along the coast and were spaced about 20 to 35 km apart; the spacing was similar between stations along each ship's track. The ships' positions relative to each other were monitored by radar during the passage, and the innermost ship obtained occasional shore fixes. Although none of the ships was equipped with satellite navigation gear, a rather accurate plotting (estimated as ± 2 km) of the tracks and station positions could be accomplished by the combination of celestial fixes and radar positioning.

Because of the relatively close spacing of the stations occupied during this survey, details of the temperature structure were revealed that were unobtainable from past work in this region. Figure 1 shows the temperature at 100 m, the approximate depth at which the strongest horizontal gradients occur. Changes in density in the Somali Basin during the southwest monsoon are, for the most part, a function of temperature, and past measurements of direct current suggest that the flow generally tends to follow in the direction of the isotherms (*3*).

Some of the results indicated by these data follow.

1) The strongest near-surface flow toward the northeast (indicated by increased gradients) lies between 6°N and 9°N, whereas the weak gradient around 5°N suggests correspondingly weak surface currents.

2) The major portion of the flow turns offshore between 7°N and 9°N but appears to do this by branching in two filaments at approximately 7°30′N and at 8°30′N.

3) To the northeast of the area where the current turns offshore a weak anticyclonic flow is found, which is similar in location to that observed in 1964 (*1*).

4) Evidence of a weak current flowing to the southwest is shown near 4°N at a depth of 100 m. Furthermore, at 300 m a weak cyclonic gyre is indicated between 4°N and 5°N; the gyre is elongated to the northeast paralleling the coast.

5) The general pattern of circulation is similar to that determined from *Argo* and

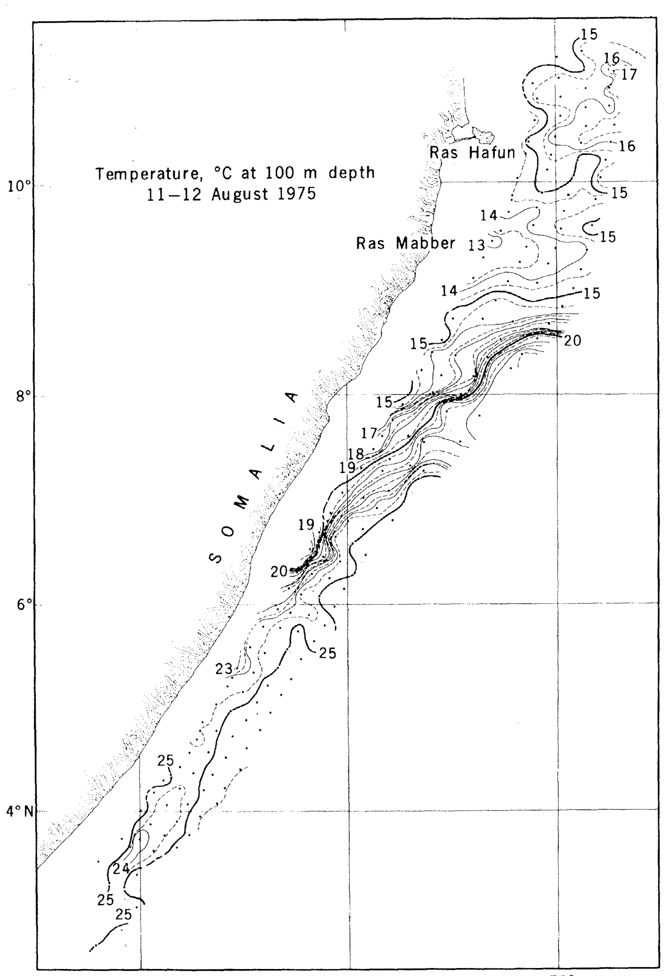

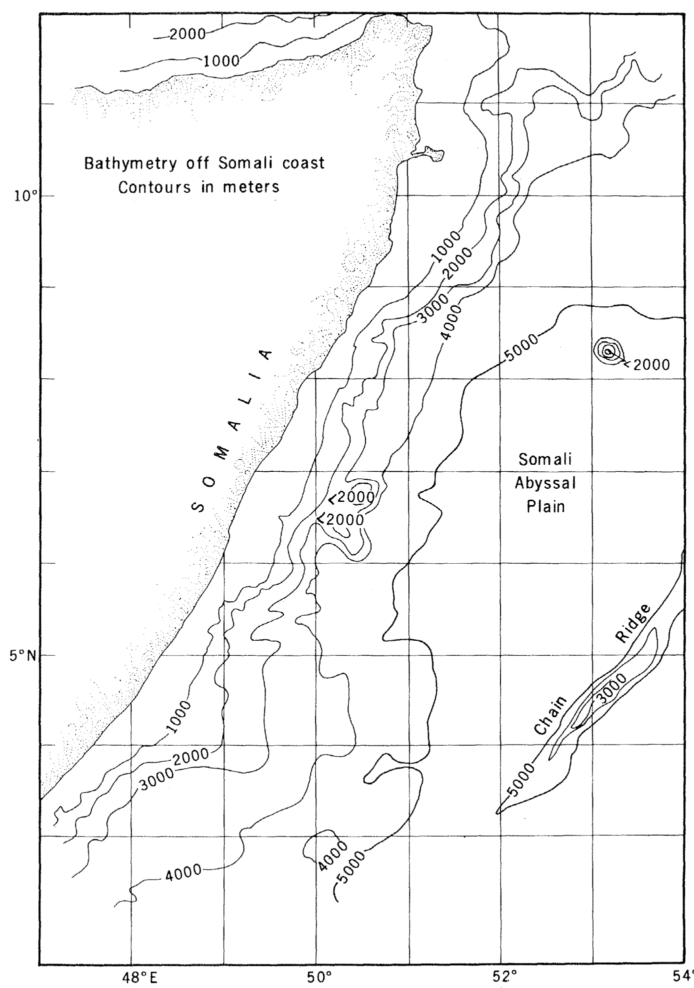

Fig. 1 (left). Map of temperature contoured at a depth of 100 m in the Somali Current at approximately maximum strength during the southwest monsoon in 1975. Dots show XBT station positions from four U.S. Navy ships traveling abreast to the northeast along the coast from Greenwich mean time 1500, 11 August, to 2300, 12 August. Fig. 2 (right). Bathymetric chart off the Somali coast based on a map by Laughton (*5*).

Discovery measurements during August 1964 (*1*) but not to that determined from *Chain* measurements during August 1970 (*3*), which showed the current turning offshore at 5°N to 6°N and a separate large gyre to the northeast of this location.

6) Small-scale meanders occur with relatively large changes in direction of the isotherms over 20 to 40 km, which suggest a degree of instability of the current alongshore before it turns offshore to the east.

7) The pronounced upwelling of cold water off Ras Mabber is also similar to that observed in 1964 (*4*).

8) Figure 2 shows the bathymetry along the Somali coast with two small seamounts at 6°25′N and 6°45′N. Although the top of each is between 1500 and 2000 m in depth, which is considerably deeper than the relatively shallow Somali Current, there is an apparent change in the flow pattern between 6°N and 7°N. A somewhat similar pattern of meandering can be observed commencing near 5°N from the 1964 temperature maps (*3*). It is quite possible, of course, that the meandering is caused by other factors, and it might be only a coincidence that it is observed in this location during these surveys.

As part of the study of the Somali Current we are now setting XBT probes from tankers paralleling the coast and hope soon to be able to monitor changes occurring throughout the entire monsoon period.

J. G. BRUCE
Woods Hole Oceanographic Institution, Woods Hole, Massachusetts 02543

References and Notes

1. J. C. Swallow and J. G. Bruce, *Deep-Sea Res.* **13**, 861 (1966).
2. J. G. Bruce, *ibid.* **15**, 665 (1968).
3. ——, *ibid.* **20**, 837 (1973). In figure 5 of this paper it should be noted that where the isotherms turn offshore to the northeast, particularly between 7°N and 9°N, the surface current vectors at some stations are 15° to 20° to the left of the isotherms.
4. ——, *J. Mar. Res.* **32**, 419 (1974).
5. A. S. Laughton, ECU map reference No. 1, National Institute of Oceanography, Godalming, Surrey, England.
6. Supported by ONR contract ONR N00014-74-C-0262, NR083-004, and NSF grant ATM74-22226 A01. Thanks are due to the U.S. Naval officers and men who put forth considerable effort in acquiring the data, especially to LtCdr Charles Martinek, U.S. Naval Academy, who supervised the data collection and helped with the data reduction. Woods Hole Oceanographic Institution contribution No. 3876.

14 January 1977

Estimates of Cenozoic Oceanic Sedimentation Rates

Abstract. *Estimation of average Cenozoic sedimentation rates for the Atlantic, Indian, and Pacific oceans indicates global synchronous fluctuations. Paleocene–early Eocene and late Eocene–early Miocene rates are only a fraction of middle Eocene and middle Miocene–Recent rates. These changes must reflect significantly different modes of continental weathering, which may be due to alternate states of atmospheric circulation marked by reduction of global precipitation.*

Estimates of the average rates of sedimentation in the Atlantic, Pacific, and Indian oceans have been prepared from data on cores recovered by the Deep Sea Drilling Project (DSDP). To prepare the estimates, the average sedimentation rate and average carbonate content for each of the 13 unequal Cenozoic time increments were calculated for each site where such values could be determined.

The data analyzed were provided by DSDP from their lithologic data bank at Scripps Institution of Oceanography. The information in the data bank has been compiled from original records and from published DSDP reports (*1*). The data we used came from 334 sites (Atlantic, 110 sites; Pacific, 170; Indian, 54). The 13 Cenozoic time increments are those chosen by Premoli-Silva *et al.* (*2*) for the preliminary atlas of the results of the DSDP. The age boundaries assigned to them for this calculation are as follows (in million years before present): Pleistocene, 0 to 2; late Pliocene, 2 to 4; early Pliocene, 4 to 6; late Miocene, 6 to 11; middle Miocene, 11 to 14; early Miocene, 14 to 22; late Oligocene, 22 to 32; early Oligocene, 32 to 38; late Eocene, 38 to 45; middle Eocene, 45 to 49; early Eocene, 49 to 54; late Paleocene, 54 to 59; and early Paleocene, 59 to 64.

Rates are expressed in meters per million years since analysis (*3*) shows that, for the purposes of gross comparison, the effects of compaction can be ignored. Precise comparison would demand rates expressed as mass per unit area per unit time.

The sedimentation rate for each of the increments at each site was determined according to the following rules.

1) If sediment representing a time increment is bounded by the adjacent increment both above and below, and if coring and biostratigraphy permitted both boundaries to be known exactly, the thickness is the interval between the upper and lower boundaries of the increment.

2) If, because of a coring gap or uncertain biostratigraphy, the exact position of one or both of the boundaries is not known, but sediment of the adjacent time increments is present, the position of each boundary is estimated as the midpoint of the interval of uncertainty; the thickness of the unit is then the interval between the midpoint of an interval of uncertainty and an exactly known point or another midpoint of an interval of uncertainty.

3) If sediment older than Pleistocene is exposed on the sea floor at a particular drill site, all the thickness of sediment representing all time increments younger than that exposed on the sea floor is reckoned to be zero.

4) If sediment of one time increment rests directly by hiatus or unconformity on sediment of a time increment older than that immediately preceding it, the thickness of sediment of all missing increments is reckoned to be zero.

5) If sediment of a time increment rests directly on igneous or metamorphic rock considered to be basement, the thickness of sediment is reckoned to be the interval from the contact with the superjacent unit to the basement rock.

6) The thickness of sediment representing a time increment is reckoned to be indeterminate if the contacts with adjacent units cannot be determined exactly or estimated by the midpoint method; indeterminate thicknesses were not used in calculating the average rates.

The carbonate sedimentation rates were estimated by multiplying the average sedimentation rate for each increment by the average carbonate value for each increment.

As shown in Fig. 1, data from the Atlantic, Pacific, and Indian oceans produce very similar curves. The correspondence between Atlantic and Pacific curves is almost perfect. The Indian Ocean curve deviates slightly, but has the same inflection points and trends. Despite the admittedly large scatter in the original data, the general trends and the similarities between the oceans are unmistakable.

It might be suggested that the curves in Fig. 1 are an artifact of either a bias of the core recovery process or the age scale used. However, we have checked this rather thoroughly, and if there is a core recovery bias, it would tend to even out differences in sedimentation rates. Similarly, the age scale would not have a significant effect on the curves unless the generally accepted radiometric ages for Cenozoic epochs are wrong by a factor of 2 to 3 for either the entire pre- or post-middle Miocene.